ChemComm

Near-infrared fluorescent HaloTag ligands for efficient organelle labelling in live cells

Journal:	*ChemComm*
Manuscript ID	CC-COM-09-2024-005144.R1
Article Type:	Communication

ChemComm

COMMUNICATION

Near-infrared fluorescent HaloTag ligands for efficient organelle labelling in live cells

Yoshiki Tanaka,[a] Masayasu Taki*[b] and Shigehiro Yamaguchi*[ab]

[¥¥^Received 00th January 20xx,
Accepted 00th January 20xx

DOI: 10.1039/x0xx00000x

A series of HaloTag ligands that incorporate near-infrared (NIR)-emissive phospha-rhodamine (POR) dyes has been developed. The PORs that contain dealkylated amino groups exhibit a hypsochromic shift in their absorption and emission wavelengths. Subsequent refinement of the POR spirocyclization equilibrium significantly enhanced membrane permeability, thereby leading to a substantial reduction in the time necessary for labelling. Consequently, target organelles could even be labeled at low POR dye concentrations in the tens of nM range.

Protein tagging with fluorescent proteins or fluorescent organic dyes has become an indispensable technique to comprehend intracellular biological phenomena. In particular, self-labelling protein tags, such as the HaloTag and SNAP-tag systems, are routinely used.[1–3] Hitherto, a diverse array of fluorescent protein-tag ligands has been devised for these systems,[4] where rhodamine dyes represent the most extensively used π-conjugated scaffolds. Specifically, a series of heteroatom-substituted rhodamine dyes, where the endocyclic oxygen atom of a classical rhodamine is replaced with a carbon, silicon, or phosphorus atom, are the most commonly used and have significantly advanced the field of protein labeling.[5–7] A distinctive characteristic of rhodamine dyes is the equilibrium that exists between their spirocyclic and zwitterionic forms which is responsive to environmental polarity. In polar environments, the fluorescent zwitterionic form predominates, while in non-polar environments, the ring-closed uncharged spirolactone form is stabilized. This equilibrium can be fine-tuned to impart the molecules with desirable properties for fluorescence imaging, including enhanced membrane permeability and a fluorogenic response upon target binding.[8–11] However, in contrast to oxygen- and silicon-bridged rhodamines, phospha-rhodamines (PORs), which have recently attracted attention as near-infrared (NIR)-emissive fluorophores with exceptional photostability,[12–16] have not yet been employed in labelling probes that exhibit spirocyclization. This can be ascribed to the high stability of the spirolactone form of the POR dyes that bear an *ortho*-carboxyphenyl group, due to the strong electron-withdrawing effect that the P=O-bridge exerts on the POR.[17] To address this limitation, Lavis and co-workers have implemented a perfluorination strategy on the aryl group at the 9-position of the xanthene ring to mitigate the nucleophilicity of the carboxylic acid.[9] The resulting JF_{711}-Halo demonstrated fluorescence enhancement upon reaction with HaloTag proteins, thus providing high-contrast images of the

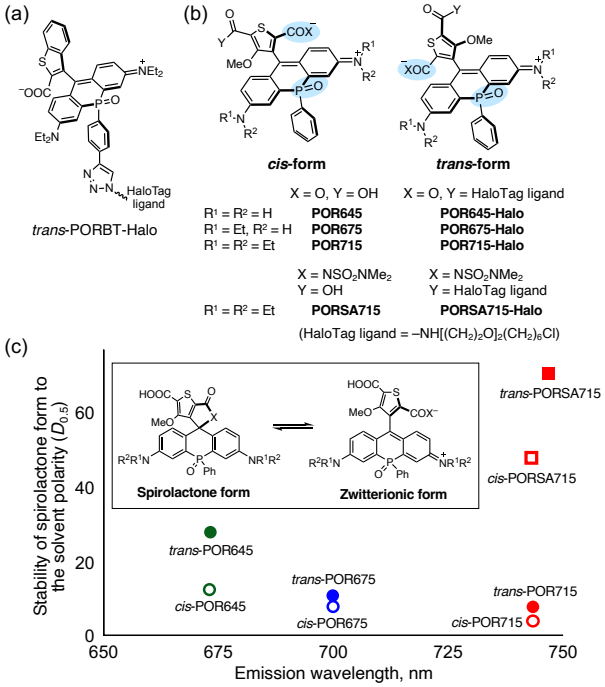

Fig. 1 (a) Structure of *trans*-PORBT-Halo. (b) Structures of a series of POR dyes bearing a thienyl ring synthesized in this work. (c) Structure–property relationship in the POR dyes. Equilibrium between the spirolactone and zwitterionic forms is shown in the inset.

[a] *Department of Chemistry, Graduate School of Science and Integrated Research Consortium on Chemical Sciences (IRCCS), Nagoya University, Furo, Chikusa, Nagoya 464-8602, Japan.*
[b] *Institute of Transformative Bio-Molecules (WPI-ITbM), Nagoya University, Furo, Chikusa, Nagoya 464-8601, Japan. E-mail: taki.masayasu.s8@f.gifu-u.ac.jp, yamaguchi@chem.nagoya-u.ac.jp*
† Electronic Supplementary Information (ESI) available. See DOI: 10.1039/x0xx00000x

target. As an alternative approach, we have recently reported the POR-based HaloTag ligand *trans*-PORBT-Halo, wherein a benzothiophene ring was introduced to the rhodamine skeleton (Fig. 1a).[17] The increase in angle strain caused by the five-membered ring destabilizes the spirolactone form, resulting in an intense emission upon target labelling. While the sterically hindered benzothiophene moiety effectively reduced reactivity toward GSH and enhanced the chemical stability in living cells, *trans*-PORBT-Halo exhibited excessive hydrophobicity, which is considered practical for imaging applications due to the benzene-annulation and the presence of a triazole ring for modification with a HaloTag ligand. This resulted in lower labelling efficiency compared to a tetramethylrhodamine-based HaloTag ligand (TMR-Halo), leading to pronounced non-specific labelling in cells expressing low levels of the HaloTag proteins.

In this study, we have developed a series of POR dyes that bear a 2,5-dicarboxy-4-methoxythiophen-3-yl group, which undergo spirocyclization in response to environmental polarity and that exhibit high chemical stability against intracellular nucleophiles (Fig. 1b). We successfully optimized the absorption and emission wavelengths, as well as polarity sensitivity (defined as $D_{0.5}$,[5] the dielectric constant of a water/dioxane mixture at which the normalized absorbance (A/A_{water}) is 0.5), by altering the number of alkyl substituents on the amino groups at either terminus of the rhodamine skeleton (Fig. 1c). These derivatives, conjugated with a HaloTag ligand, were employed for live cell monitoring of organelle dynamics in time-lapse and super-resolution imaging using stimulated emission depletion (STED) microscopy. Furthermore, we demonstrated a significant improvement in cell staining capability upon replacing the 2-carboxy group on the thiophene ring with a sulfonamide, thus enabling efficient labelling of the target organelles with at low probe concentrations in the tens of nM range.

The synthesis of the POR derivatives with a pendant thiophene ring, *i.e.*, POR645, POR675, and POR715, is shown in Scheme S1 (ESI†). For the synthesis of POR645 and POR675, the amino groups of the phospha-xanthone were protected with a trimethylsilyl (TMS) and an allyl group, respectively, prior to reaction with the corresponding aryllithium reagent. Consistent with a previous report, due to the high rotational energy barrier of the bond between the carboxythiophene and xanthene rings, all POR dyes were obtained as a mixture of stereoisomers, including isomers wherein the carboxy and P=O groups were orientated *cis* and *trans* to each other.[17] These isomers were separated using reversed-phase HPLC and their configurations were determined via ^{1}H NMR spectroscopy. Namely, in light of the comparison in the NMR spectra for the previously reported PORBT,[17] an isomer that showed the chemical shift of the ortho protons on the *P*-phenyl group in the lower magnetic field was assigned to the trans isomer, while the other isomer to be the cis isomer. The trans isomer thus assigned showed a higher R_f value in the TLC (SiO_2) than that of the cis isomer due to the smaller dipole moment of the former isomer (Fig. S1, ESI†). This trend is consistent with the observation for PORBT.

The photophysical properties of the POR dyes were evaluated in 50 mM HEPES buffer at pH 7.4. All compounds showed intense absorption and emission bands in the far-red to NIR region, indicating the formation of the zwitterionic structure in aqueous solution (Fig. 2 and Figs. S3–S4 in ESI†). A reduction in the number of *N*-alkyl groups in the PORs led to a decrease in the highest occupied molecular orbital (HOMO) energy level, resulting in a hypsochromic shift of both the absorption and emission maxima (Table 1). The fluorescence quantum yields of POR675 and POR715 (Φ_F = 0.12–0.13) are comparable to that of *trans*-PORBT-Halo, while POR645 exhibited a comparatively low Φ_F of 0.03–0.05. However, no significant differences in the photophysical properties were observed between the respective *trans* and *cis* isomers. To better understand the relationship between the structure and the spirocyclization equilibrium, the absorption spectra were measured in mixed solvent of water and dioxane with varying composition ratios, and their $D_{0.5}$ values were determined (Fig. 3 and Fig. S5 in ESI†).[18] As the water content decreased, the coloured zwitterionic forms underwent ring-closing to form the colourless spirocyclic structures. Of the six PORs tested, *cis*-POR715 demonstrated the greatest propensity for ring-opening ($D_{0.5}$ < 5), while *trans*-POR645 exhibited the highest $D_{0.5}$ value (27.4), indicating pronounced stability of the spirolactone form. The observed variations in the $D_{0.5}$ values among the isomers were attributed to differences in the amplitude of their dipole moments, whereby the *cis* isomer possesses a larger dipole moment than the *trans* isomer.

Subsequently, we evaluated the chemical stability of the PORs against physiological nucleophiles. In contrast to POR715, regardless of its stereochemistry, a decrease in the intensity of the absorption and emission bands was observed at pH 10 for POR645 and POR675, with a pronounced effect observed for POR645 (Figs. S6–S8, ESI†). The appearance of a new absorption

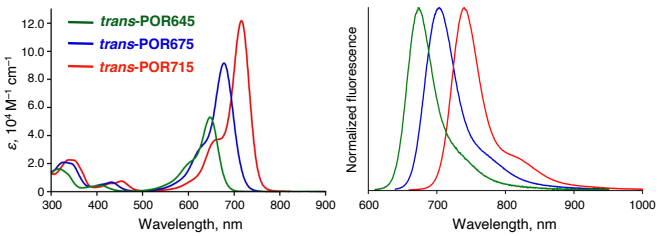

Fig. 2 Absorption (left) and normalized fluorescence (right) spectra of *trans*-POR645 (green), *trans*-POR675 (blue), and *trans*-POR715 (red) in 50 mM HEPES buffer (pH = 7.4).

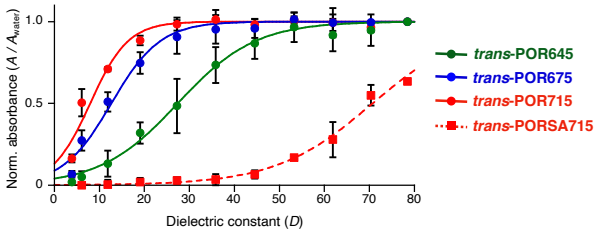

Fig. 3 Normalized absorbance (A/A_{water}) of each dye in water-dioxane mixtures (v/v, 5–100%) as a function of the dielectric constant. A_{water} represents the absorbance in 100% water at the chosen wavelength. For *trans*-PORSA715, A_{water} is assumed to be identical to that of *trans*-POR715. *trans*-POR645 (green circle, solid line), *trans*-POR675 (blue circle, solid line), *trans*-POR715 (red circle, solid line), *trans*-PORSA715 (red square, dashed line). Curves were obtained by sigmoidal fitting of the data (for details, see the ESI†). Error bars show the standard deviation (n = 3–5).

Table 1. Photophysical properties of phospha-rhodamines in PBS (pH 7.4)

POR dye	λ_{abs} / nm	$\varepsilon \times 10^4$ / M^{-1} cm^{-1}	λ_{em} / nm	Φ_{FL}[a]	$D_{0.5}$[c]
trans-POR645	648	5.30[b]	674	0.03	27.4
cis-POR645	645	6.97[b]	674	0.05	16.9
trans-POR675	678	9.15	704	0.13	12.7
cis-POR675	674	8.56	703	0.15	8.3
trans-POR715	716	12.2	740	0.12	8.0
cis-POR715	714	9.62	740	0.13	3.6
trans-PORSA715	720	7.74	747	0.10	70.7
cis-PORSA715	714	9.30	740	0.12	47.2
trans-PORBT[d]	716	8.65	742	0.08	12.1
cis-PORBT[d]	714	10.20	739	0.11	7.3

[a] Absolute fluorescence quantum yields. [b] Measured in acidic buffer (pH 4). [c] Dielectric constant at which A/A_{water} is 0.5. [d] From ref 17.

band in the absorption around 500 nm suggests that the π-conjugation system is disrupted by deprotonation of the amino groups. The stability toward GSH followed a similar trend (Figs. S10–S12, ESI†), where a significant decrease in the absorption and emission bands of POR645 was observed. This phenomenon was attributed to the Michael addition of GS^- to the highly electrophilic dealkylated POR fluorophore. It should be noted here that a POR715 derivative without a methoxy group on the thiophene ring exhibits high reactivity toward GSH (Fig. S14, ESI†). This finding clearly confirms the effective protective role that the 9-position of the xanthene ring palys against nucleophilic attack, thereby enhancing chemical stability. Despite certain limitations of POR645 with the low Φ_F values and high pH-sensitivity, all the PORs, including their isomers, could be conjugated with a HaloTag ligand.

The resulting *cis* and *trans* isomers of POR645, POR675, and POR715 were employed to stain live HeLa cells expressing the HaloTag fusion protein on the targeted organelles, the nucleus, microtubules, mitochondria, and endoplasmic reticulum (ER) (Figs. S19–S24, ESI†). Following appropriate incubation methods and subsequent washing with a dye-free medium, fluorescent images were acquired using a confocal laser scanning microscope equipped with a 730 nm or 640 nm excitation laser. It should be noted that, to stain the cells with POR675-Halo and POR645-Halo, 10 μM verapamil, well-known inhibitor of drug efflux pump proteins, was added to the incubation media. In all cases, the cells exhibited distinct staining patterns pertaining to the targeted organelles without any detectable nonspecific staining. This result stands in sharp contrast with those obtained previously for *cis*/*trans*-PORBT-Halo, which demonstrated stereochemistry-selective membrane permeability; specifically, the *trans* isomer was capable of labelling the targets while the *cis* isomer was accumulated in the lipid bilayer.[17] The improvement in the organelle labelling ability can be clearly ascribed to the reduced hydrophobicity of the thiophene-modified POR dyes.

The absorption and emission characteristics of POR675 make it appropriate for STED microscopy at a depletion wavelength of 775 nm (Fig. S26, ESI†). In contrast, it was not feasible to use POR715 for STED microscopy due to the direct excitation of POR715 by the depletion laser (Fig. S27, ESI†). Moreover, to demonstrate the practical utility of *trans*-POR675

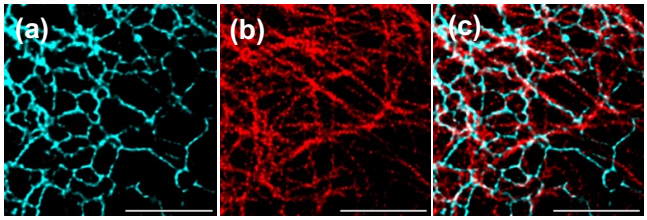

Fig. 4 STED image of a live COS-7 cell expressing KDEL-Halo after incubation with (a) *trans*-POR675-Halo and (b) SiR-tubulin for 4 h. The merged image is shown in (c). λ_{ex} = 670 nm; λ_{STED} = 775 nm; λ_{em} = 720–750 nm for *trans*-POR675-Halo; λ_{em} = 600–600 nm for SiR-tubulin. Scale bar = 5 μm.

in two-colour STED imaging, cells expressing KDEL-Halo were labelled with *trans*-POR675-Halo and SiR-tubulin, a commercially available microtubule fluorescent probe (Fig. 4). Image acquisition was performed on two channels, 600–660 nm and 720–750 nm for the SiR and POR675 fluorophores, respectively, where excitation occurred at 670 nm and depletion at 775 nm. The distinct separation of the two images with minimal crosstalk indicated the suitability of this dye combination for simultaneous STED image acquisition of cellular structures on two NIR channels. This method will be a practical tool to understand how microtubule growth and ER network remodelling are regulated at a super-resolution level.

Although all POR-based HaloTag ligands exhibited membrane permeability, achieving the maximum fluorescence intensities required almost 3 h of cell treatment with each ligand. In this regard, Johnsson *et al*. have reported that the modification of the intramolecular nucleophile with a sulfonamide group contributes to the stabilization of the membrane-permeable spirolactone forms of the dyes, resulting in the improvement of labelling efficiency.[11,19] Accordingly, we chose the most chemically stable dye, POR715, and synthesized PORSA715 and its derivative with a HaloTag ligand (PORSA715-Halo), wherein the 2-carboxy group on the thiophene ring is replaced with an *N*,*N*-dimethylsulfamide group (Fig. 1b). As expected, both the *cis* and *trans* isomers exhibited significant shifts in their spirocyclization equilibria towards the ring-closed form, resulting in larger $D_{0.5}$ values of 47.2 and 70.7, respectively (Fig. 3 and Table 1). Notably, the ε of *trans*-PORSA715-Halo was lower than that of *trans*-POR715-Halo, indicative of a propensity to form the spirocyclized structure, even in aqueous environments. Indeed, binding with isolated HaloTag protein resulted in 1.3- and 2.6-fold increases in the absorption and emission intensities, respectively, highlighting a slight fluorogenic property (Fig. S16, ESI†). Conversely, the addition of bovine serum albumin (BSA) resulted in a significant decrease in the absorption band due to its spirocyclization in a hydrophobic microenvironment (Fig. S18, ESI†).

A subsequent assessment of membrane permeability using live HeLa cells expressing hH2B-HaloTag, via time-dependent fluorescent signal tracking, demonstrated that the fluorescence intensity of *trans*-PORSA715-Halo reached a maximum around 30 min after dye addition, which represents a dramatic improvement compared to *trans*-POR715-Halo (Fig. 5a). To further evaluate its labelling efficiency, we conducted a competitive staining experiment of HeLa cells stably expressing

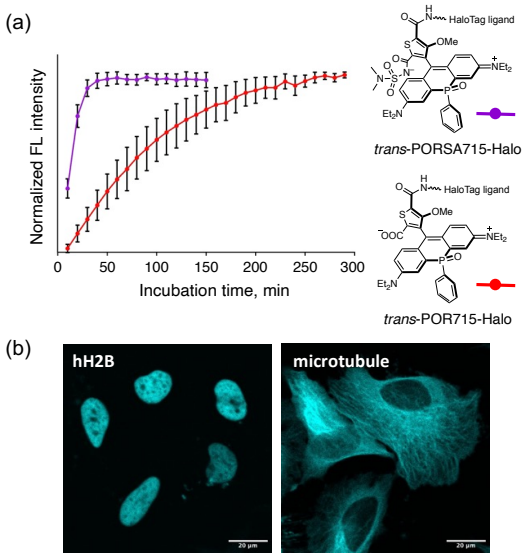

Fig. 5 (a) Normalized fluorescence intensities of *trans*-PORSA715-Halo (purple) and *trans*-POR715-Halo (red) at different time points in live HeLa cells expressing hH2B-HaloTag. Error bars show the standard deviation (n = 5). (b) Confocal images of live HeLa cells expressing HaloTag on the nucleus (left) and the microtubules (right) labelled with 10 nM *trans*-PORSA715-Halo for 2 h. λ_{ex} = 730 nm; λ_{em} = 750–790 nm. Scale bar = 20 μm.

hH2B-HaloTag with TMR-Halo, which is known for its high cell permeability (Figs. S31 and S32, ESI†). When stained with media containing identical probe concentrations, the calculated occupancy of *trans*-PORSA715-Halo and TMR-Halo in HaloTag proteins was 3:7, while the ratio dropped to 1:9 when using JF_{646}-Halo instead of *trans*-PORSA715-Halo, likely due to the enhanced cellular permeability of *trans*-PORSA715-Halo, as corroborated by comparative experiments of labelling rates (Fig. S30, ESI†). Consequently, the excellent labelling performance of *trans*-PORSA715-Halo enabled target staining under physiological conditions at a concentration as low as 10 nM in growth medium without additives (Fig. 5b).

Finally, we decided to take advantage of the high photostability and minimal perturbation to cellular functions associated with low probe concentrations, and the negligible photo-toxicity of NIR light. Thus, we performed time-lapse imaging of cell nuclei during mitosis over a period of 25 h with a frame interval of 90 s (Movie S1, ESI†), as well as video rate imaging (~30 fps) of the mitochondrial dynamics for 337 s (>10000 frames) (Movie S2, ESI†). Even after recording these images, significant decreases in the fluorescence intensity were not observed, therefore demonstrating the outstanding photostability of the *P*-rhodamine fluorophores.

In summary, a series of NIR fluorescent HaloTag ligands based on phospha-rhodamine dyes has been developed. We successfully achieved the optimization of the photophysical properties and the spirocyclization equilibrium, via modification of the substituents on the amino groups and the 2-carboxy group on the thiophene ring, thus allowing us to perform two-colour STED imaging and long-term time-lapse imaging with high temporal resolution. These POR-based labelling probes hold significant promise as chemical tools for imaging organelle networks and single-molecule tracking.

The authors are grateful to Prof. Yasushi Okada (The University of Tokyo) for kindly donating HeLa cells stably expressing hH2B-HaloTag. This work was supported by JSPS KAKENHI grants (22K19108 to MT; 22K21346 to SY; 22J23745 to YT; 22H04926 for Advanced Bioimaging Support) and JST CREST (JPMJCR21O5 to SY).

Data availability

The data supporting this article have been included as part of the ESI.†

Conflicts of interest

There are no conflicts to declare.

Notes and references

1 G. V. Los, L. P. Encell, M. G. McDougall, D. D. Hartzell, N. Karassina, C. Zimprich, M. G. Wood, R. Learish, R. F. Ohana, M. Urh, D. Simpson, J. Mendez, K. Zimmerman, P. Otto, G. Vidugiris, J. Zhu, A. Darzins, D. H. Klaubert, R. F. Bulleit and K. V. Wood, *ACS Chem. Biol.*, 2008, **3**, 373-382.
2 A. Keppler, S. Gendreizig, T. Gronemeyer, H. Pick, H. Vogel and K. Johnsson, *Nat. Biotechnol.*, 2003, **21**, 86-89.
3 C. A. Hoelzel and X. Zhang, *ChemBioChem*, 2020, **21**, 1935-1946.
4 A. Cook, F. Walterspiel and C. Deo, *ChemBioChem*, 2023, **24**, e202300022.
5 A. N. Butkevich, G. Y. Mitronova, S. C. Sidenstein, J. L. Klocke, D. Kamin, D. N. H. Meineke, E. D'Este, P-T. Kraemer, J. G. Danzl, V. N. Belov and S. W. Hell, *Angew. Chem. Int. Ed.*, 2016, **55**, 3290-3294.
6 L. Lesiak, X. Zhou, Y. Fang, J. Zhao, J. R. Beck and C. I. Stains, *Org. Biomol. Chem.*, 2020, **18**, 2459-2467.
7 J. B. Grimm, A. K. Muthusamy, Y. Liang, T. A. Brown, W. C. Lemon, R. Patel, R. Lu, J. J. Macklin, P. J. Keller, N. Ji and L. D. Lavis, *Nat. Methods*, 2017, **14**, 987-994.
8 D. Englert, E-M. Burger, F. Grün, M. S. Verma, J. Lackner, M. Lampe, B. Bühler, J. Schokolowski, G. U. Nienhaus, A. Jäschke and M. Sunbul, *Nat. Commun.*, 2023, **14**, 3879.
9 J. B. Grimm, A. N. Tkachuk, L. Xie, H. Choi, B. Mohar, N. Falco, K. Schaefer, R. Patel, Q. Zheng, Z. Liu, J. Lippincott-Schwartz, T. A. Brown and L. D. Lavis, *Nat. Methods*, 2020, **17**, 815-821.
10 N. Lardon, L. Wang, A. Tschanz, P. Hoess, M. Tran, E. D'Este, J. Ries and K. Johnsson, *J. Am. Chem. Soc.*, 2021, **143**, 14592-14600.
11 L. Wang, M. Tran, E. D'Este, J. Roberti, B. Koch, L. Xue and K. Johnsson, *Nat. Chem.*, 2020, **12**, 165-172.
12 X. Chai, X. Cui, B. Wang, F. Yang, Y. Cai, Q. Wu and T. Wang, *Chem.-Eur. J.*, 2015, **21**, 16754-16758.
13 X. Zhou, R. Lai, J. R. Beck, H. Li and C. I. Stains, *Chem. Commun.*, 2016, **52**, 12290-12293.
14 M. Grzybowski, M. Taki, K. Senda, Y. Sato, T. Ariyoshi, Y. Okada, R. Kawakami, T. Imamura and S. Yamaguchi, *Angew. Chem. Int. Ed.*, 2018, **57**, 10137-10141.
15 X. Chai, J. Xiao, M. Li, C. Wang, H. An, C. Li, Y. Li, D. Zhang, X. Cui and T. Wang, *Chem.-Eur. J.*, 2018, **24**, 14506-14512.
16 M. Grzybowski, M. Taki, K. Kajiwara and S. Yamaguchi, *Chem.-Eur. J.*, 2020, **26**, 7912-7917.
17 Q. Wu, M. Taki, Y. Tanaka, M. Kesherwani, Q. M. Phung, S. Enoki, Y. Okada, F. Tama and S. Yamaguchi, *Angew. Chem. Int. Edit.*, 2024, **63**, e202400711.
18 F. E. Critchfield, J. A. Gibson and J. L. Hall, *J. Am. Chem. Soc.*, 1953, **75**, 1991-1992.
19 L. Wang, J. Hiblot, C. Popp, L. Xue and K. Johnsson, *Angew. Chem. Int. Ed.*, 2020, **59**, 21880-21884.

Data availability

The authors confirm that the data supporting the findings of this study are available within the article and the ESI.